

How robust is a thermal photon interpretation of the ALICE low- p_T data?

M. Klasen,^a C. Klein-Bösing,^{b,c} F. König^a and J. P. Wessels^b

^a*Institut für Theoretische Physik, Westfälische Wilhelms-Universität Münster,
Wilhelm-Klemm-Straße 9, D-48149 Münster, Germany*

^b*Institut für Kernphysik, Westfälische Wilhelms-Universität Münster,
Wilhelm-Klemm-Straße 9, D-48149 Münster, Germany*

^c*ExtreMe Matter Institute, GSI, Planckstraße 1, D-64291 Darmstadt, Germany*

E-mail: michael.klasen@uni-muenster.de,

c.klein-boesing@uni-muenster.de, f.koenig@uni-muenster.de,

j.wessels@uni-muenster.de

ABSTRACT: We present a rigorous theoretical analysis of the ALICE measurement of low- p_T direct-photon production in central lead-lead collisions at the LHC with a centre-of-mass energy of $\sqrt{s_{NN}} = 2.76$ TeV. Using NLO QCD, we compute the relative contributions to prompt-photon production from different initial and final states and the theoretical uncertainties coming from independent variations of the renormalisation and factorisation scales, the nuclear parton densities and the fragmentation functions. Based on different fits to the unsubtracted and prompt-photon subtracted ALICE data, we consistently find $T = 304 \pm 58$ MeV and 309 ± 64 MeV for the effective temperature of the quark-gluon plasma (or hot medium) at $p_T \in [0.8; 2.2]$ GeV and $p_T \in [1.5; 3.5]$ GeV as well as a power-law (p_T^{-4}) behavior for $p_T > 4$ GeV as predicted by QCD hard scattering.

Contents

1	Introduction	1
2	Partonic subprocesses	3
3	Nuclear parton density uncertainties	5
4	Fragmentation function uncertainties	8
5	Direct-photon production in heavy-ion collisions	10
6	Conclusions	14
A	Prompt-photon yields and their uncertainties in NLO QCD	15

1 Introduction

One of the goals of the physics program at the CERN Large Hadron Collider (LHC) is the study of deconfined, strongly interacting matter, which existed in the early universe and which can today be re-created and investigated in heavy-ion collisions. An important probe for this so-called quark-gluon plasma (QGP) are photons emitted from the deconfined partons before thermalisation, in the thermal bath, during expansion and cooling of the QGP, and finally from the thermal hadron gas. The transverse momentum distribution of these photons can be used to estimate the temperature of the system, although the exact interpretation is complicated by these different phases, the radial expansion, more generally the temporal evolution of phase space, and co-existing states of matter. Experimentally, an effective temperature is usually extracted from an exponential fit to the excess of direct-photon production at low transverse momentum (p_T) above the expectation from vacuum production.

In Ref. [1], the first observation of a low- p_T direct-photon signal at the LHC has been reported by the ALICE collaboration.¹ There, an inverse slope parameter of $T_{\text{LHC}} = 304 \pm 51$ MeV has been extracted from an exponential fit to the photon spectrum in central (0-40%) lead-lead collisions at $\sqrt{s_{NN}} = 2.76$ TeV and low transverse momenta of $p_T \in [0.8; 2.2]$ GeV. The inverse slope parameter of this measurement is significantly higher than the one obtained previously by the PHENIX collaboration in 0-20% central gold-gold collisions with $\sqrt{s_{NN}} = 200$ GeV at RHIC, which resulted in $T_{\text{RHIC}} = 221 \pm 19 \pm 19$ MeV [2]. The latter

¹In nuclear collision experiments, photons originating from meson decays are usually distinguished from *direct* photons. The latter are divided into *thermal* and non-thermal *prompt* (plus medium-induced) photons, and these again into photons produced *directly* in the hard collision and those coming from quark and gluon *fragmentation*. The double use of the word *direct* can sometimes lead to confusion.

was higher than the transition temperature to the QGP of about $T_{\text{crit}} = 170$ MeV, but 1.5 to 3 times smaller than the initial temperature T_0 of the dense matter due to the space-time evolution following its initial formation; in hydrodynamical models, which describe the data at $\sqrt{s_{NN}} = 200$ GeV, T_0 ranges from 600 to 300 MeV depending on the formation time, assumed to lie between $\tau_0 = 0.15$ and 0.6 fm/ c [3].

The two general-purpose LHC experiments ATLAS and CMS have also recently measured prompt-photon production in lead-lead collisions at $\sqrt{s_{NN}} = 2.76$ TeV with $p_T > 40$ and 20 GeV, respectively [4, 5]. In this transverse momentum range, photons (like electroweak Z and W bosons [6, 7]) are expected to be dominantly produced in hard partonic collisions and to be unaffected by the strongly interacting medium, so that they can be described with next-to-leading order (NLO) QCD programs such as JETPHOX [8].

However, photons from electromagnetic decays of neutral mesons (mostly $\pi^0, \eta \rightarrow \gamma\gamma$) must first be removed using meson data [1], Monte Carlo simulations [2] and/or by applying an isolation criterion, which e.g. limits the energy of all other particles in a cone of size $R_{\text{iso}} = \sqrt{\Delta\eta^2 + \Delta\phi^2} < 0.3$ or 0.4 around the photon to $E_T(R_{\text{iso}}) < 6$ or 5 GeV [4, 5]. The remaining “prompt” photon sample then still contains both direct photons, produced at tree-level through the processes $q\bar{q} \rightarrow \gamma g$ and $qg \rightarrow \gamma q$, and photons emitted in the collinear fragmentation of quarks and gluons produced in partonic scattering processes. Isolation criteria also reduce the contribution of fragmentation photons, since these are generally produced inside a high- p_T jet of hadrons. The separation of these direct and fragmentation photons becomes ambiguous, i.e. scheme- and scale-dependent, at NLO of perturbative QCD, but their interplay and the factorisation of the associated infrared singularities have been studied intensively theoretically [9]. As a result, NLO calculations describe very well prompt-photon production in pp collisions at the LHC with $\sqrt{s} = 7$ TeV down to $p_T \geq 21$ GeV [10–13].

At smaller transverse momenta, a transition from hard to thermal photon production is expected to occur in central heavy-ion collisions, in contrast to peripheral heavy-ion and pp collisions. For this reason, the transverse momentum distribution of inclusive photons has been measured by the ALICE collaboration in lead-lead collisions at $\sqrt{s_{NN}} = 2.76$ TeV from 16 GeV down to 0.4 GeV. In addition, the same has been done in pp collisions at $\sqrt{s} = 7$ TeV down to 0.3 GeV. In both cases, contributions from decay photons were subtracted using neutral pion data and transverse mass (m_T) scaling [14]. The data for the 0-40% most central heavy-ion collisions showed a clear deviation from the perturbative QCD prediction below p_T -values of 4 GeV which was not observed for pp and peripheral (40-80%) heavy-ion collisions [1]. Similar observations had been made in a preceding analysis of the PHENIX collaboration in minimum bias, 0-20% and 20-40% central gold-gold collisions at RHIC with $\sqrt{s_{NN}} = 200$ GeV [2].

In this paper we will scrutinise the thermal photon interpretation of the ALICE low- p_T data with respect to theoretical uncertainties in the perturbative QCD prediction. Not only do these uncertainties arise from variations of the renormalisation and factorisation scales in the incoming and outgoing hadrons and photons, which have so far only been varied simultaneously by a factor of two about the photon p_T , but they are also caused by uncertainties in the factorisation scheme [15], the nuclear parton density functions (nPDFs)

and the photon fragmentation functions (FFs).

Nuclear PDFs are subject to intrinsic uncertainties of the proton PDFs, in particular of the gluon [16], and cold nuclear modification effects, such as nuclear shadowing [17]. Both are expected to be significantly larger at the LHC with its small values of partonic momentum fractions $x \simeq 2p_T/\sqrt{s_{NN}} \simeq 10^{-3}$ than at RHIC and at low scales of $\mu_f \simeq p_T \simeq 2$ GeV rather than at large scales. Extra p_T -broadening (the Cronin effect) is expected to become small at high (RHIC and LHC) centre-of-mass energies and small x [18]. The latter has been confirmed experimentally at RHIC by the measurement of direct photons in d +Au reactions [19] and at the LHC via the comparison of charged hadron production in proton-proton and proton-nucleus collisions [20]. In general, when going from proton-proton to nucleus-nucleus collisions, one must also account for isospin suppression of prompt-photon production due the presence of neutrons (126) and not only protons (82) in the lead nucleus. This is, however, mostly relevant in the valence-quark region at large x . Saturation effects appear to set in only at very small values of x . The influence of these effects has been analysed in several global fits of nPDFs [21–24].

The photon fragmentation functions are also subject to considerable uncertainties, in particular the one for gluons. In the absence of sufficiently detailed experimental data from e^+e^- collisions, they are typically modeled on vector meson fragmentation [25]. As an alternative, it has been proposed to use slightly virtual photons decaying into low-mass lepton pairs, as these do not have fragmentation contributions and need not be isolated experimentally [26–28].

The remainder of this paper is organised as follows: In Sec. 2, we will study the relative importance of the different partonic subprocesses contributing to prompt photon production in lead-lead collisions. Sections 3 and 4 give a brief review of the current uncertainty on the nuclear PDFs and photon FFs. Our main results are presented in Sec. 5, where we compare our NLO QCD predictions to the ALICE data and estimate the total theoretical uncertainty coming from the various sources defined above. Our conclusions are given in Sec. 6. For future use, we present in App. ?? our NLO QCD calculations for the invariant prompt-photon yields in tabular form.

2 Partonic subprocesses

As stated in the introduction, the goal of this paper is to test how robust a thermal photon interpretation of the low- p_T ALICE data is. We will explore to what extent the observed excess of photons with transverse momenta below 4 GeV can be explained by the production of hard photons in the initial partonic collision alone, taking into account all theoretical uncertainties.

The production of these photons is calculated perturbatively in NLO QCD using JET-PHOX 1.2 [8]. As is well known, the truncation of the perturbative series at this order leads to an artificial dependence on the unphysical renormalisation scale μ and the initial- and final-state factorisation scales μ_f and μ_D . These have so far been varied only simultaneously, and we will later vary them also individually by a factor of two around the central scale p_T . In addition, uncertainties in the determination of the PDFs must also be taken

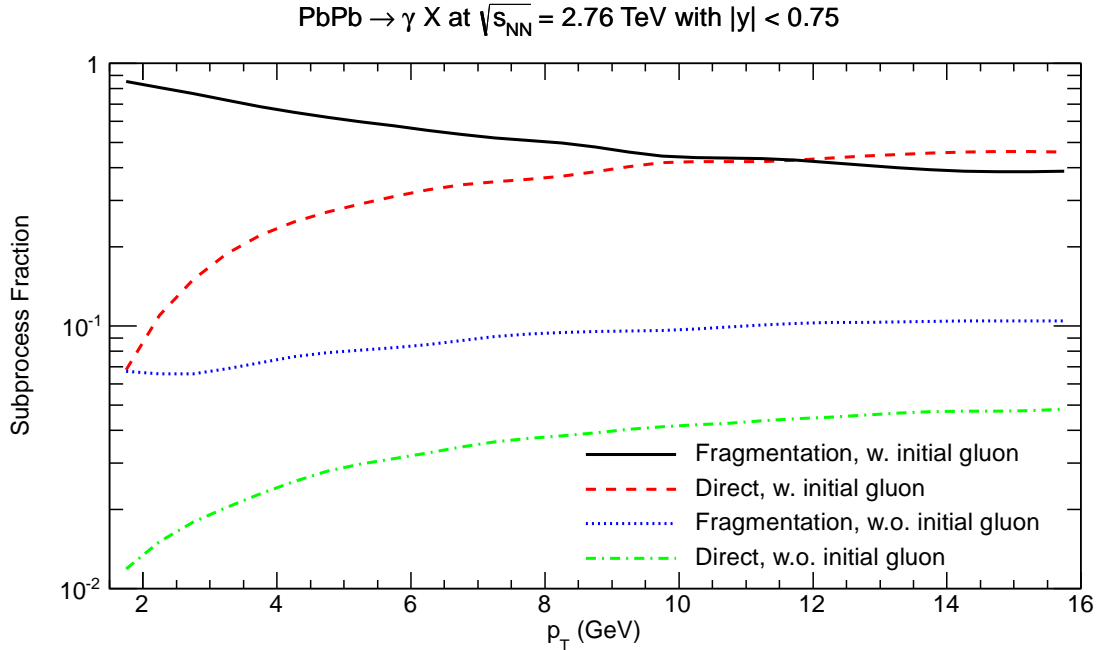


Figure 1. Relative contributions to the total NLO prompt-photon cross section in lead-lead collisions with a center-of-mass energy of $\sqrt{s_{NN}} = 2.76$ TeV. We show individually the fragmentation (full) and direct (dashed) subprocesses with initial gluons as well as those with initial quarks and antiquarks only (dotted and dot-dashed).

into account, and in the case of heavy-ion collisions not only for the free-proton PDFs, but also for their nuclear modification, which is commonly parametrised as a modification factor $R_{i/A}(x, \mu_f)$ of the density for parton i . Furthermore, at low transverse momenta and in the absence of a photon isolation criterion, fragmentation processes are expected to dominate, thus introducing an additional uncertainty from the photon fragmentation function.

Before we address these sources of uncertainty in the following chapters, it is illustrative to learn about the relative contributions of the various partonic subprocesses leading to prompt-photon production in lead-lead collisions. These depend in particular on the momentum fractions x and z of the partons in the PDFs $f(x, \mu_f)$ and FFs $D(z, \mu_D)$, but also on the factorisation scales μ_f and μ_D . Since we are interested in the low- p_T region, we set these scales here to 2 GeV, which is already in the perturbative regime, but only slightly larger than the starting scale $Q_0 \sim 1.3$ GeV [21–24]. The relevant momentum fractions in the initial state can be computed from the photon’s transverse momentum by $x_T = 2p_T/\sqrt{s_{NN}}$ (the true x at central rapidity), leading to typical values of $x_T \sim 10^{-3}$. Our simulations show that the momentum fractions in the final-state fragmentation range from $z \sim 0.01$ (0.1) to 1 at $p_T = 2$ (16) GeV. In this section, we use the best fit of EPS09 [21] for the nPDFs and the BFG set II [25] for the FFs as our baseline.

In Fig. 1, we plot the relative contributions to the total NLO prompt-photon cross section in lead-lead collisions with $\sqrt{s_{NN}} = 2.76$ TeV. Individually shown are the fragmentation (full) and direct (dashed) subprocesses with initial gluons as well as those with

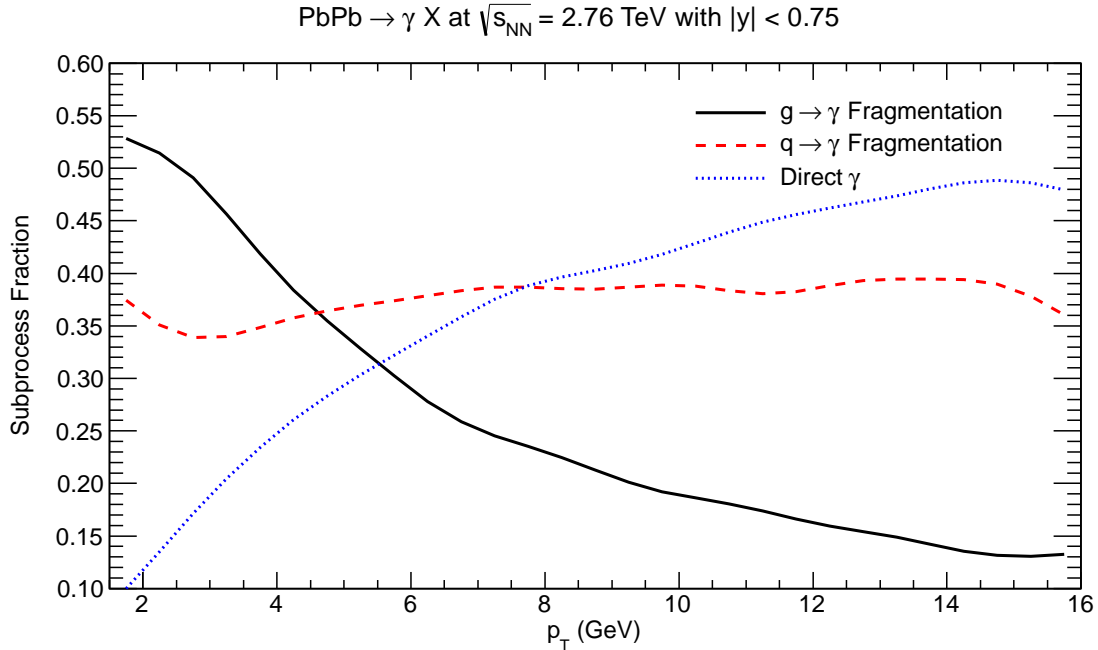


Figure 2. Relative final-state contributions to the total NLO prompt-photon cross section in lead-lead collisions with $\sqrt{s_{NN}} = 2.76$ TeV. We show individually the gluon (full) and quark (dashed) fragmentation subprocesses as well as the direct subprocesses (dotted).

initial quarks and antiquarks only (dotted and dot-dashed). As expected, fragmentation contributions dominate at low transverse momenta (up to 12 GeV), i.e. over almost the entire p_T -range measured by ALICE. Only at larger transverse momenta the direct QCD “Compton” process $qg \rightarrow \gamma g$ takes over. In the initial state, the gluon contribution dominates in fact throughout, while pure quark and antiquark initial states make up for at most ten percent. We therefore expect the uncertainty on the gluon in bound nucleons at small x to play an important role.

Looking at the final state, we plot in Fig. 2 the subprocesses with gluon (full) and quark (dashed) fragmentation as well as the direct subprocesses (dotted). As can be seen, the very low- p_T region (below 4 GeV) is dominated by gluon fragmentation into photons, which is very poorly constrained experimentally. Quark fragmentation gives an almost constant contribution of about 40% over the entire p_T -range. Direct photons become larger than quark fragmentation at transverse momenta of 8 GeV and than all fragmentation processes above 12 GeV (see above).

3 Nuclear parton density uncertainties

In this paper, we use the EPS09 nPDFs as our baseline [21]. There, the bound-proton PDFs are defined in terms of nuclear modifications $R_{i/A}(x, \mu_f)$ applied to CTEQ6.1M [16] free-proton PDFs $f_{i/p}(x, \mu_f)$,

$$f_{i/A}(x, \mu_f) \equiv R_{i/A}(x, \mu_f) \cdot f_{i/p}(x, \mu_f). \quad (3.1)$$

The bound-neutron PDFs are obtained by assuming isospin symmetry. E.g. the total up-quark (u) distribution per nucleon in a nucleus A with Z protons is

$$f_{u/A}(x, \mu_f) = \frac{Z}{A} [R_{u/A}^v f_{u/p}^v + R_{u/A}^s f_{u/p}^s] + \frac{A-Z}{A} [R_{d/A}^v f_{d/p}^v + R_{d/A}^s f_{d/p}^s], \quad (3.2)$$

where d corresponds to the down-quark and the superscripts v and s refer to valence and sea quark contributions, respectively. The parametrisation of the nuclear modifications $R_{i/A}(x, \mu_f)$ is performed at the charm quark mass (m_c) threshold imposing the momentum and baryon number sum rules

$$\sum_{i=q,\bar{q},g} \int_0^1 dx x f_{i/A}(x, m_c) = 1, \quad \int_0^1 dx [f_{u/A}^v(x, m_c) + f_{d/A}^v(x, m_c)] = 3, \quad (3.3)$$

for each nucleus A separately. At higher scales, the nPDFs are obtained by solving the DGLAP evolution equations. This approach results in an excellent fit to the different types of nuclear hard-process data [21], suggesting that factorisation works well in the energy range studied and that the extracted nPDFs are universal in the region $x \geq 0.005$, $\mu_f \geq 1.3$ GeV.

The theoretical uncertainties of the free-proton PDFs are obtained using the 40 error sets of the CTEQ6.1M parametrisation [16]. An additional 30 error sets are assigned pairwise to the uncorrelated eigendirections of the 15 parameters fitted to the nuclear collision data sets. A total uncertainty band at 90% confidence level is then calculated from the 71 sets defined by fixing either $R_{i/A}(x, \mu_f)$ to the best fit value and varying the free-proton PDFs or fixing the latter to its best fit value and varying the former. These variations then contribute pairwise to the size of the upper and lower errors via

$$\delta^+ f = \sqrt{\sum_i [\max(f_i^{(+)} - f_0, f_i^{(-)} - f_0, 0)]^2}, \quad (3.4)$$

$$\delta^- f = \sqrt{\sum_i [\max(f_0 - f_i^{(+)}, f_0 - f_i^{(-)}, 0)]^2}. \quad (3.5)$$

As the authors acknowledge, this factorised approach represents a simplification, violating, e.g., in some cases momentum conservation, so that strictly speaking the free- and bound-proton PDF uncertainty analyses should not be separated [21].

Note that the minimal value of $x = 0.005$ constrained by experimental data in the EPS09 fit lies above the value of $x = 0.001$ expected to be relevant for the low- p_T ALICE data. The nPDFs therefore rely in this region on an extrapolation from higher x -values. Experimental data down to $x = 5 \cdot 10^{-5}$ exist from the BRAHMS collaboration [29], who have measured charged-hadron production at forward rapidity $\eta = 2.2$ and 3.2 in pp and $d+\text{Au}$ collisions at $\sqrt{s_{NN}} = 200$ GeV. However, they have not been included in any of the nPDFs and would in fact lead to a poor description by the EPS09 fits, in particular for transverse momenta below 2 GeV at $\eta = 2.2$ and below 4 GeV at $\eta = 3.2$ (see Fig. 14 in [21]).

In order to estimate the bias from different underlying free-proton PDFs, parametrisations of the nuclear modification, and fitted nuclear data sets, we also study the best fits

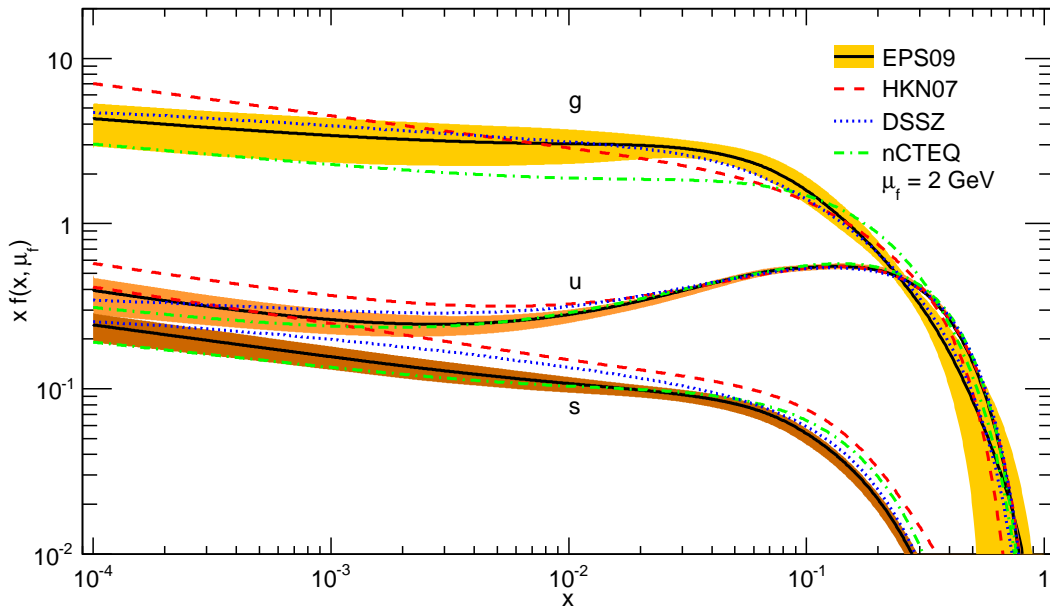


Figure 3. Nuclear parton distribution functions (nPDFs) of gluons, up (\sim down) and strange quarks in lead ions from the best fits of different collaborations [21–24], at the factorisation scale $\mu_f = 2$ GeV. The uncertainty band is only shown for the EPS09 group [21].

of the HKN07 [22], DSSZ [23] and nCTEQ [24] collaborations. In particular, the HKN07 nPDFs are based on the MRST1998 free-proton set [30] and those of DSSZ on the more recent MSTW2008 set [31]. The nCTEQ parametrisation is (so far) the only one that does not rely on a factorisation into a nuclear modification factor and free-proton PDFs. Instead it introduces an explicit A -dependence in the coefficients of the x -dependent functional form of the PDFs at the starting scale. So only the technical framework of the CTEQ6M analysis is used here [32].

In Fig. 3, we plot the total parton densities defined in Eqs. (3.1) and (3.2) for protons bound in lead ions and as obtained in the EPS09 (full) [21], HKN07 (dashed) [22], DSSZ (dotted) [23] and nCTEQ (dot-dashed) [24] fits. As it is usually done, we plot x times the nPDF, i.e. the momentum distribution of the partons in the bound proton. Error bands are only shown for the EPS09 analysis. In descending order of importance, the gluon, up- and strange-quark densities are shown separately. Those for down quarks differ only very little from the up-quark densities, mostly in the valence (large- x) region, and are not shown separately. Whereas the up- (and down-) quark densities show the characteristic valence behavior and dominate at large x , the gluon density becomes already dominant for x -values below 0.2 and in particular by more than an order of magnitude in the low- x region around 10^{-3} relevant for the prompt-photon data at low p_T . The uncertainty estimated by EPS09 amounts there to almost a factor of two. Our calculations show that the uncertainty due to the proton PDF alone accounts for less than half of the uncertainty. If also the other parametrisations are taken into account in order to eliminate the theoretical bias, the uncertainty increases to more than a factor of two, due in particular to the different

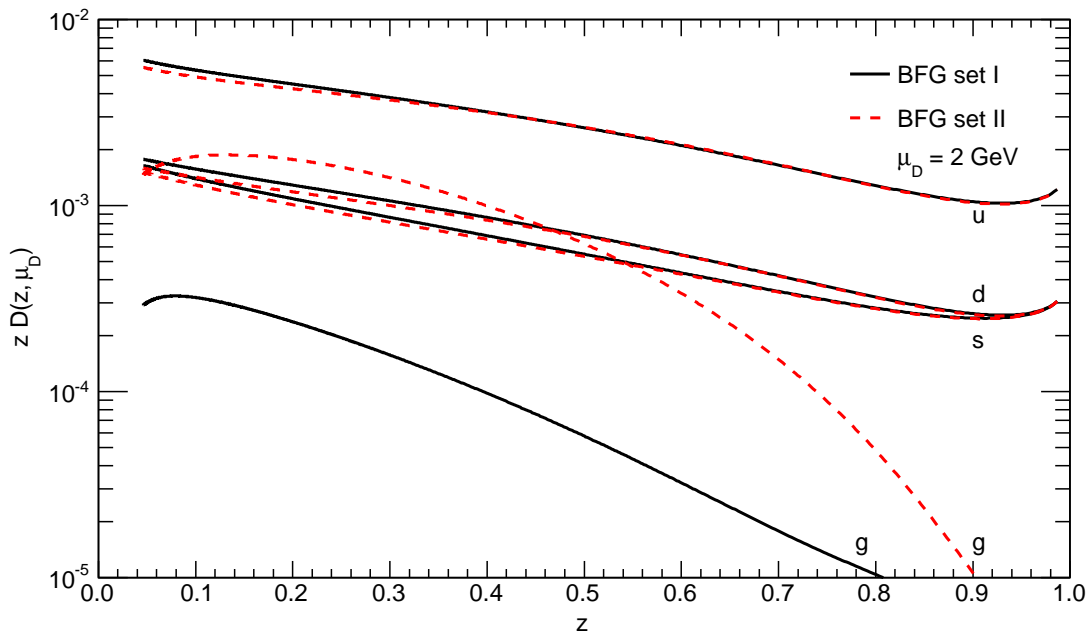


Figure 4. Photon fragmentation functions (FFs) for up, down and strange quarks as well as for gluons by the BFG collaboration [25] at the factorisation scale $\mu_f = 2$ GeV. The two sets differ in particular with respect to the gluon.

shapes of the HKN07 and nCTEQ gluon fits. We stress again that we are considering here a region of extrapolation, where no experimental constraints are taken into account. In the sea-quark region at low x , the up- and strange-quark densities follow roughly the shape of the gluon as expected, but are smaller by about an order of magnitude. The uncertainties for the up quark (and down quark) are somewhat smaller than those of the gluon. This is probably due to better constraints on the large- x (valence) region, which influence the low- x region through the sum rules. However, the uncertainty for the strange quark amounts again to at least a factor of two. We therefore expect a considerable impact of the nPDF uncertainties, in particular from the gluon and from the different parametrisations, on the description of the low- p_T prompt photon data.

4 Fragmentation function uncertainties

Fragmentation photons typically contribute less than 20% to the total yield in fixed-target experiments, but can become dominant at collider energies, in particular at low transverse momenta and in the absence of isolation criteria, as shown in Sec. 2. Note that the removal of any isolation criterion is imperative in the search for thermal photon sources in heavy-ion collisions. The hadronic input needed for the non-perturbative fragmentation functions would best be determined from inclusive photon production in e^+e^- annihilation, but unfortunately the experimental data are very limited and are furthermore dominated by the pointlike quark-photon fragmentation function. Therefore, all existing parametrisations use vector-meson dominance to model the photon fragmentation at low scales. The

two most recent BFG parametrisations have, e.g., been obtained from ALEPH and HRS data on ρ production [25]. They leave a large uncertainty in the gluon fragmentation to photons, which is parametrised with the two sets I and II. Heavy quarks are included above their production thresholds with zero boundary conditions.

Fig. 4 shows the FFs as obtained in the two BFG sets. Again, we show the momentum distribution, i.e. z times the FF $D(z, \mu_D)$ with $\mu_D = 2$ GeV as the factorisation scale. In descending size, the up-, down- and strange-quark FFs are shown separately, together with the one for the gluon. Due to its larger charge ($e_u = +2/3$), which enters quadratically, the up-quark contribution exceeds the one for down and strange quarks with charge $e_d = e_s = -1/3$ by about a factor of four. The difference between down and strange quarks is due to quark mass effects. The gluon is very weakly constrained (essentially only by the momentum sum rule), and its uncertainty amounts to almost an order of magnitude. Only when comparing the ratio of gluon and up-quark FFs into pseudoscalar mesons to the one into vector mesons and assuming that they should be of the same order due to the reduction of non-perturbative effects, BFG come to the conclusion that set II may be preferable. As is customary, we have followed BFG in this choice for our baseline, but stress again that the uncertainty on the gluon FF into photons remains large.

Despite the fact that photons are colour-neutral objects, they may also be affected by final-state effects, similarly, but perhaps not quite as strongly as mesons. In particular, the fragmentation of partons into photons is expected to be sensitive to the presence of a strongly interacting medium, since the final partons produced in the hard collision undergo multiple scattering and suffer energy loss from multiple-gluon radiation during the fragmentation process. This is usually modeled by rescaling the energy in a medium-modified fragmentation function [33]

$$zD_{\gamma/d}(z, \mu_D) = \int_0^{k_\perp(1-z)} d\varepsilon P_d(\varepsilon, k_\perp) z^* D_{\gamma/d}(z^*, \mu_D), \quad (4.1)$$

where $z^* = z/(1 - \varepsilon/k_\perp)$ and where $P_d(\varepsilon, k_\perp)$ denotes the probability that the leading parton d with energy k_\perp has lost an energy ε in the medium. The soft-gluon emission is usually assumed to follow a Poisson distribution. Alternatively, an improved Double Log Approximation (DLA) [34], the Modified Leading-Log Approximation (MLLA) [35], or parton shower and hadronisation models in Monte Carlo generators can be employed.

One would expect the modification of the fragmentation function to be largest for low values of the momentum fraction z , where its hadronic component is most important, just as the photon structure function is dominated by its hadronic component at low x [36]. As discussed above, the values of z probed in the ALICE experiment range from $z \sim 0.01$ (0.1) to 1 at $p_T = 2$ (16) GeV, i.e. we expect the largest modification at low values of p_T . This is also confirmed by a simple argument about the fragmentation time, which can be estimated with $\hbar/\mu_D \geq 0.1$ fm/c for $p_T \leq 2$ GeV and thus becomes comparable to the formation time of the QGP $\tau_0 = 0.15 \dots 0.6$ fm/c [3] only at low values of p_T .

Since nothing is known experimentally about light vector-meson (in particular ρ) fragmentation in the medium (and very little *in vacuo*, see above), one must resort to pseudoscalar (pion) fragmentation. It is then possible to simulate both initial- (isospin effects,

shadowing) and final-state effects on inclusive photon production and compare, e.g., to PHENIX data [37]. The fragmentation modification is then found to be strongest at low values of p_T (down to 4 GeV), but the experimental errors are still too large to identify it unambiguously. It has therefore been proposed to study not only inclusive photon production, but also photon-pion correlations to improve the separation of initial- and final-state effects [33].

5 Direct-photon production in heavy-ion collisions

In this section, we compute the transverse-momentum distribution of prompt (non-thermal) photons in NLO QCD and compare them to the experimental data for direct photons (not coming from decays) of the ALICE collaboration. Particular emphasis is put on the theoretical errors coming from the different sources described above, i.e. an individual variation of the renormalisation and factorisation scales by a factor of two up and down the central value p_T , the nuclear PDFs from the EPS09 fits as described in Sec. 3, and the FFs from the BFG I and II fits as described in Sec. 4. Our goal is to establish to what extent the excess of the direct-photon data over the perturbative QCD prediction survives, once it is subtracted and all theoretical errors are taken into account, and how this procedure and these errors affect the determination of the effective temperature of the QGP.

In Fig. 5 we compare the transverse-momentum distribution of the ALICE data obtained in central (0-40%) lead-lead collisions at $\sqrt{s_{NN}} = 2.76$ TeV (black data points [1]) to our NLO QCD predictions for prompt photons (red) as well as their fragmentation (blue) and direct (green) contributions. The centrality of the collision enters our calculations as an overall normalisation factor [38]

$$\langle T_{\text{PbPb}} \rangle_{0-40\%} \equiv \frac{\int_{b_{\min}}^{b_{\max}} d^2b T_{\text{PbPb}}}{\int_{b_{\min}}^{b_{\max}} d^2b}, \quad (5.1)$$

which relates the invariant differential cross section $E d^3\sigma/dp^3 = d\sigma/(2\pi \Delta y p_T dp_T)$ (after integration over the azimuthal angle $\int d\phi = 2\pi$ and for a finite rapidity interval $|y| < 0.75$) to the invariant yield through [38]

$$\frac{1}{2\pi N_{\text{ev}}} \frac{dN}{\Delta y p_T dp_T} = \langle T_{\text{PbPb}} \rangle_{0-40\%} \frac{d\sigma}{2\pi \Delta y p_T dp_T}. \quad (5.2)$$

If we use for Eq. (5.1) the integration boundaries and averaging integrals of the ALICE experiment given in Tab. 1 of Ref. [39], we find $\langle T_{\text{PbPb}} \rangle_{0-40\%} = 13 \text{ mb}^{-1}$. If we then apply this normalisation to our theoretical predictions for the transverse-momentum spectrum in Fig. 5 (color) and compare to the experimental data (black) in the highest measured p_T bin ($8 \text{ GeV} < p_T < 11 \text{ GeV}$), we find very good agreement as expected in this perturbative region.

It is well known that the fragmentation contribution (blue) is considerably softer in p_T than the direct contribution (green), i.e. the former falls off much more steeply than the latter. In Fig. 5, the fragmentation contribution dominates in all significant p_T -bins,

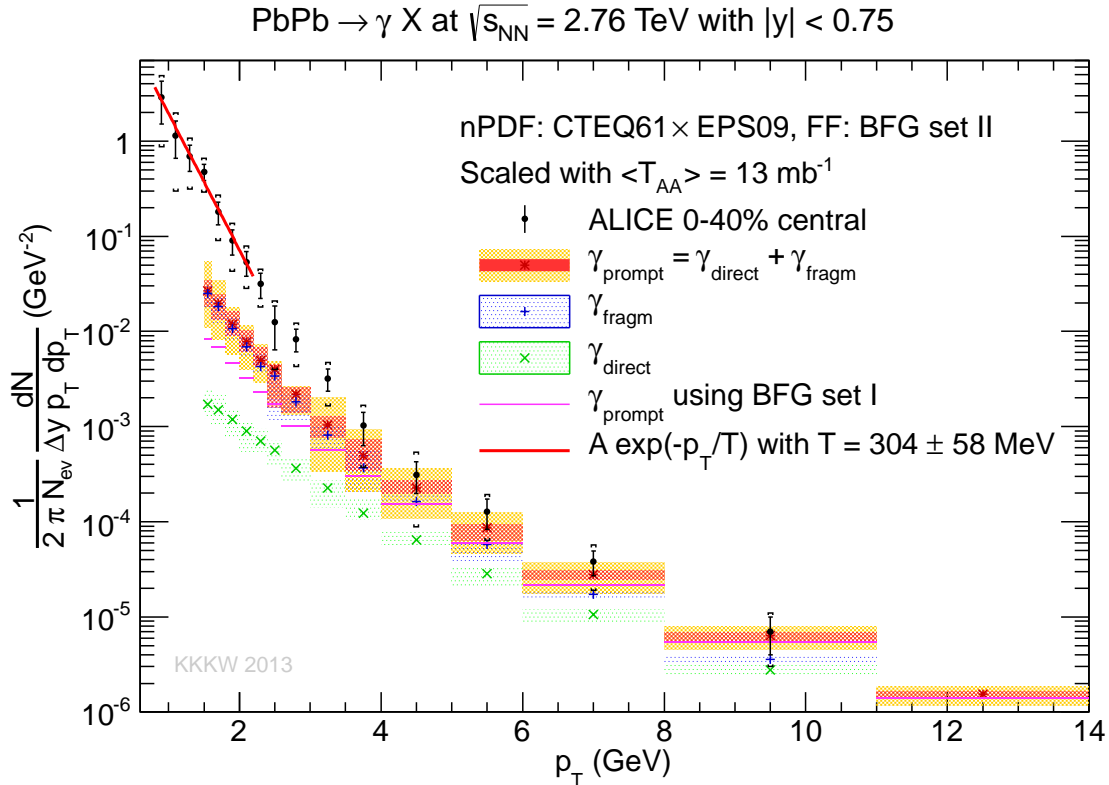


Figure 5. Transverse-momentum distribution of direct photons in central (0-40%) lead-lead collisions at $\sqrt{s_{NN}} = 2.76$ TeV (black data points [1]) compared to our NLO QCD predictions for prompt photons (red) as well as their fragmentation (blue) and direct (green) contributions. Independent scale (yellow) and nPDF (red/blue/green) uncertainties as well as the FF variation (magenta) are shown separately, as are the statistical (vertical bars) and systematic (horizontal brackets) experimental errors.

and in the lowest p_T -bins it is more than an order of magnitude larger than the direct contribution. This leads to a large uncertainty from the fragmentation function. E.g., in the lowest p_T -bins the theoretical prediction with BFG I FFs (magenta) is about a factor of three smaller than the one with BFG II FFs (blue). On the basis of BFG I FFs, one would thus attribute a larger excess to thermal photon production than with BFG II FFs. In the higher p_T -bins, the FF uncertainty is smaller due to the larger contributions of both direct and quark-fragmentation photons (see Sec. 4).

The scale variation uncertainty (yellow) also turns out to be important. When all three scales are varied individually, the cross section changes by more than a factor of two up and down, much more than if all scales would be varied simultaneously. For low scales, where the cross section is larger, one would thus attribute a smaller excess to thermal photon production. Note that for $p_T < 3$ GeV, we vary the factorisation scales only from p_T to $2p_T$ to stay above the nPDF and FF starting scales, which means that the true scale uncertainty there is even larger than the one shown. Only at larger values of p_T , the scale uncertainty becomes eventually smaller. It could in principle be reduced by resumming the

logarithmic parts of the higher-order corrections to all orders. This has been attempted, but unfortunately the corresponding codes for transverse-momentum [40] and joint [41, 42] resummation are not publicly available. The low- p_T region is furthermore known to be sensitive to the Gaussian smearing parameters entering the non-perturbative factor required there [43].

The uncertainties arising from the nPDFs (red, green and blue bands) are less important than the FF and scale errors, but are still well visible in Fig. 5. Their relative size remains constant over many low- p_T bins, corresponding to low momentum fractions x of the partons in the lead nucleus and the shadowing and free gluon density uncertainties present there, but eventually also becomes somewhat smaller at larger p_T or x . This was expected from Sec. 3, since the shadowing and gluon uncertainties are smaller and the quark contribution is larger at higher values of x . As the nPDF fits by the other collaborations mentioned in Sec. 3 mostly fall within the EPS09 uncertainty band, we do not show the corresponding predictions here.

Considering statistical (vertical bars) and systematic (horizontal brackets) experimental as well as all theoretical errors described above *individually*, we find a photon excess (i.e. non-overlapping error bars) for $p_T < 2.4$ GeV and the bin $2.6 \text{ GeV} < p_T < 3.0$ GeV, i.e. at smaller p_T -values than the ALICE collaboration, which did not take into account theoretical uncertainties, but used a larger theoretical normalisation (see Fig. 6 of Ref. [1]). Fitting this excess in the range $0.8 \text{ GeV} < p_T < 2.2$ GeV with an exponential form $A \exp(-p_T/T)$, we find an inverse slope parameter of $T = 304 \pm 58$ MeV (304 ± 51 GeV in Ref. [1]), where our (slightly larger) error has been obtained by adding statistical and systematic errors in quadrature and where both turn out to contribute with equal weight. Note, however, that these results have been obtained from data which include still both thermal and prompt photon contributions.

The thermal (plus medium-induced) photon production rate alone can be estimated by first subtracting from the experimental data the theoretically computed prompt photon contribution and then fitting again the exponential slope of the difference. This can, however, only be done for p_T values larger than the starting scales of the nPDFs and FFs. In Fig. 6, the data points (full circles) now show the difference of data versus theory. The error bars have been obtained by propagating statistical and systematic experimental errors as well as scale and nPDF errors in quadrature. This leads to an additional photon excess in the bin $3.0 \text{ GeV} < p_T < 3.5$ GeV. The (discrete) FF uncertainty is estimated by performing the same procedure with the (less favoured) BFG I fit (open circles) instead of the BFG II fit. Here, only the experimental errors were taken into account. Nevertheless, it falls within the total error of the other uncertainties.

Since the limitation of the previous fit to $p_T < 2.2$ GeV is somewhat arbitrary, we perform two fits to the differential data points in Fig. 6. The first one for $1.5 \text{ GeV} < p_T < 2.2$ GeV (blue) includes only data points from the overlap of the experimentally fitted and our theoretically calculated p_T -bins. As the data point in the lowest p_T -bin is somewhat higher than the three data points below and above it (see Fig. 5), this fit leads to a lower effective temperature of 255 ± 99 MeV (263 ± 96 MeV for BFG I FFs). Within its larger error, it is, however, still in agreement with the unsubtracted fit value of 304 ± 58 MeV obtained

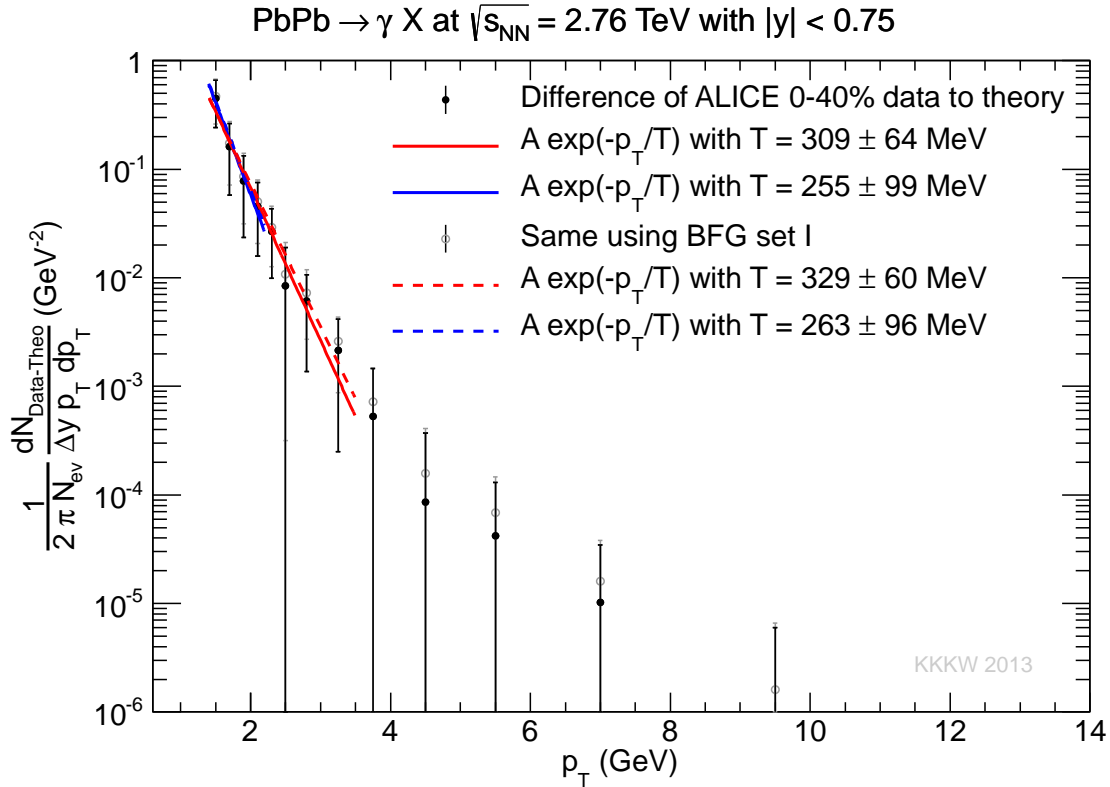


Figure 6. Difference of experimental direct-photon and theoretical prompt-photon yields using BFG II (full circles) and BFG I (open circles) FFs with all other errors added in quadrature. Also shown are exponential fits to the points up to $p_T < 2.2$ GeV (blue) and 3.5 GeV (red).

above. If we include all data points that show a non-zero difference from prompt-photon production, i.e. $1.5 \text{ GeV} < p_T < 3.5 \text{ GeV}$, we find instead $309 \pm 64 \text{ MeV}$ ($329 \pm 60 \text{ MeV}$ for BFG I FFs), which is again much closer to the unsubtracted fit value. The additional data points thus counterbalance the weight of the first one and bring the result into good agreement with the one based on Fig. 5.

This result may at first sight seem surprising and coincidental. One must, however, take into account the relative size of the prompt-photon contribution, which falls off like p_T^{-4} as predicted by our calculations, to the measured direct-photon rate in the different p_T regions, shown in Fig. 7. Indeed, we find that prompt photons contribute less than 20% for $p_T < 2.4 \text{ GeV}$ (less than 10% for BFG I FFs), i.e. their subtraction and the theoretical error do not strongly modify the exponential fall-off of the experimental data in this region. Above 4 GeV, we find instead an almost constant ratio of prompt over direct photons that is consistent with one within the uncertainties, i.e. these observed photons are produced in hard scatterings. In the intermediate region, it was already clear from Fig. 5 that the prompt-photon contribution is substantial, larger than 20% (10% for BFG I FFs), and must indeed first be subtracted from the experimental data. Only then can the excess be described again by an exponential fit, which we found to be in good agreement with the fit to the unsubtracted data at low p_T .

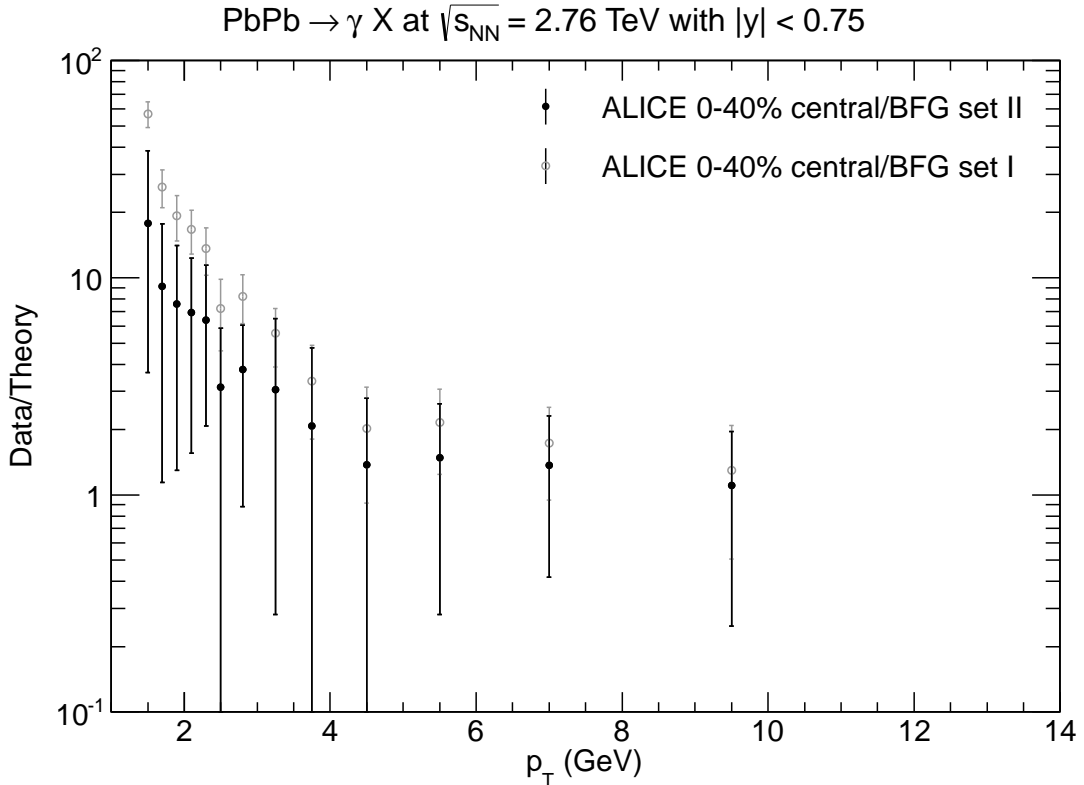


Figure 7. Ratio of experimental direct-photon and theoretical prompt-photon yields using BFG II (full circles) and BFG I (open circles) FFs with all other errors added in quadrature.

Several attempts have been made to describe the transition from thermal to hard photons in the intermediate p_T region theoretically. E.g., bremsstrahlung from a fast charged parton may be induced by the medium [44], or a hard quark or gluon and a thermal parton may convert to a hard photon through annihilation or QCD Compton scattering [45]. As discussed above, we found that current data can well be described by an exponential fit up to $p_T < 3.5$ GeV, once the prompt-photon contribution is subtracted. If we include the data points above p_T values of 3.5 GeV, we obtain a very similar effective temperature of 319 ± 66 MeV, as these data points no longer carry much statistical weight. An almost identical effective temperature of 311 ± 64 MeV is also obtained when we vary all scales simultaneously instead of individually. This clearly demonstrates that the scale variation error is strongly correlated among different p_T -bins. It affects mostly the normalisation constant A rather than the inverse slope parameter T .

6 Conclusions

In conclusion, we have performed in this work a first rigorous theoretical analysis of the ALICE measurement of direct-photon production in central lead-lead collisions with a centre-of-mass energy of $\sqrt{s_{NN}} = 2.76$ TeV at low values of p_T of 0.8 to 14 GeV. Based on a next-to-leading order QCD calculation, we found that prompt photon production in this

region was largely induced by initial gluons and dominated by fragmentation contributions (for $p_T < 4$ GeV those of a final gluon) due to the absence of an isolation criterion. This resulted in large theoretical uncertainties from independent variations of the renormalisation and factorisation scales, nuclear parton densities and fragmentation functions.

Nevertheless, we were able to confirm that the experimental data are well fitted in the region $p_T \in [0.8; 2.2]$ GeV by an exponential form $A \exp(-p_T/T)$ with an effective temperature of $T = 304 \pm 58$ MeV, with a slightly larger uncertainty than the 51 MeV quoted by the ALICE collaboration. The reason is that in this region prompt photons contribute less than 10 to 20% to the total direct photon rate, so that their subtraction and theoretical error do not influence the fit result very much. We also verified that already for values of $p_T > 4$ GeV the experimental data fall off with p_T^{-4} as predicted by perturbative QCD. In this region, the theoretical uncertainty is under reasonable control and strongly correlated among the different p_T -bins, in particular the one coming from the scale variation.

In the intermediate p_T -region from 1.5 to 3.5 GeV, the prompt-photon contribution had to be subtracted from the experimental data before a sensible exponential fit could be performed. We were able to verify an exponential fall-off with a very similar effective temperature of 309 ± 64 MeV. This result did not change significantly when extended to p_T values of 7 GeV or when all scales were varied simultaneously, confirming the strong correlation of the theoretical error among different p_T bins. Based on current ALICE data, a global thermal description thus seems to hold also in the intermediate p_T region, and the presence of additional mechanisms, such as medium-induced bremsstrahlung and/or thermal parton conversion, do not need to be invoked to reproduce the measured photon spectra.

A Prompt-photon yields and their uncertainties in NLO QCD

For future use, we present in Tab. 1 our NLO QCD calculations for the invariant prompt-photon yield in central (0-40%) lead-lead collisions at $\sqrt{s_{NN}} = 2.76$ TeV and their uncertainties as a function of transverse momentum in tabular form. All numbers have been rescaled according to Eq. (5.2) using $\langle T_{PbPb} \rangle_{0-40\%} = 13 \text{ mb}^{-1}$.

Acknowledgments

The work of C. Klein-Bösing was supported by the Helmholtz Alliance Program of the Helmholtz Association, contract HA216/EMMI “Extremes of Density and Temperature: Cosmic Matter in the Laboratory”. We thank the ALICE collaboration for making their preliminary data available to us and J.P. Guillet, J. Owens, W. Vogelsang and M. Wilde for useful discussions.

p_T (GeV)	BFG set II	PDF error		Scale error		Fragm.	Direct	BFG set I
		+	-	+	-			
1.5 - 1.6	2.68e-02	7.2e-03	8.4e-03	2.8e-02	1.6e-02	2.51e-02	1.71e-03	8.39e-03
1.6 - 1.8	1.98e-02	4.7e-03	6.4e-03	1.4e-02	1.1e-02	1.83e-02	1.51e-03	6.90e-03
1.8 - 2.0	1.19e-02	4.3e-03	2.8e-03	5.9e-03	6.2e-03	1.07e-02	1.19e-03	4.66e-03
2.0 - 2.2	7.77e-03	2.4e-03	1.7e-03	3.7e-03	3.8e-03	6.87e-03	8.99e-04	3.22e-03
2.2 - 2.4	4.96e-03	1.9e-03	6.8e-04	2.3e-03	2.0e-03	4.26e-03	7.05e-04	2.32e-03
2.4 - 2.6	3.98e-03	5.0e-04	2.4e-03	8.7e-04	2.0e-03	3.41e-03	5.68e-04	1.72e-03
2.6 - 3.0	2.20e-03	3.6e-04	7.8e-04	4.4e-04	8.5e-04	1.83e-03	3.66e-04	1.01e-03
3.0 - 3.5	1.04e-03	2.5e-04	2.7e-04	1.0e-03	7.0e-04	8.15e-04	2.27e-04	5.73e-04
3.5 - 4.0	4.94e-04	2.4e-04	1.5e-04	4.4e-04	2.9e-04	3.70e-04	1.23e-04	3.06e-04
4.0 - 4.5	2.87e-04	7.4e-05	3.6e-05	1.8e-04	1.5e-04	2.09e-04	7.80e-05	1.91e-04
4.5 - 5.0	1.72e-04	3.0e-05	2.5e-05	9.6e-05	9.0e-05	1.19e-04	5.22e-05	1.21e-04
5.0 - 5.5	1.09e-04	9.8e-06	4.0e-05	4.6e-05	5.2e-05	7.33e-05	3.53e-05	7.37e-05
5.5 - 6.0	6.58e-05	1.2e-05	1.5e-05	3.5e-05	2.8e-05	4.35e-05	2.23e-05	4.64e-05
6.0 - 6.5	4.65e-05	7.4e-06	5.6e-06	1.5e-05	2.0e-05	3.01e-05	1.64e-05	3.49e-05
6.5 - 7.0	3.05e-05	6.1e-06	3.1e-06	1.3e-05	1.0e-05	1.87e-05	1.18e-05	2.50e-05
7.0 - 7.5	2.28e-05	1.4e-06	7.7e-06	5.8e-06	8.6e-06	1.42e-05	8.55e-06	1.71e-05
7.5 - 8.0	1.50e-05	3.5e-06	1.5e-06	7.0e-06	4.4e-06	8.50e-06	6.54e-06	1.31e-05
8.0 - 8.5	1.21e-05	9.5e-07	2.3e-06	3.5e-06	3.8e-06	7.12e-06	4.94e-06	9.84e-06
8.5 - 9.0	8.74e-06	1.0e-06	1.5e-06	1.9e-06	2.7e-06	5.16e-06	3.59e-06	7.31e-06
9.0 - 9.5	6.47e-06	1.6e-06	9.8e-07	2.1e-06	1.8e-06	3.51e-06	2.97e-06	5.78e-06
9.5 - 10.0	5.00e-06	1.6e-06	3.8e-07	1.3e-06	1.4e-06	2.68e-06	2.31e-06	4.42e-06
10.0 - 10.5	4.10e-06	4.4e-07	7.0e-07	1.0e-06	1.1e-06	2.16e-06	1.94e-06	3.58e-06
10.5 - 11.0	3.13e-06	6.0e-07	2.9e-07	7.8e-07	7.1e-07	1.75e-06	1.38e-06	2.71e-06
11.0 - 11.5	2.48e-06	3.0e-07	3.1e-07	5.1e-07	6.5e-07	1.30e-06	1.17e-06	2.28e-06
11.5 - 12.0	2.00e-06	2.7e-07	3.3e-07	4.9e-07	5.0e-07	1.08e-06	9.21e-07	1.76e-06
12.0 - 12.5	1.63e-06	3.5e-07	3.1e-08	4.2e-07	3.5e-07	8.40e-07	7.92e-07	1.45e-06
12.5 - 13.0	1.36e-06	7.9e-08	2.4e-07	2.5e-07	3.1e-07	6.96e-07	6.61e-07	1.23e-06
13.0 - 13.5	1.13e-06	3.5e-08	2.9e-07	2.0e-07	3.0e-07	5.72e-07	5.53e-07	1.03e-06
13.5 - 14.0	8.89e-07	2.2e-07	1.3e-07	2.4e-07	1.8e-07	4.57e-07	4.32e-07	8.29e-07
14.0 - 14.5	7.78e-07	9.2e-08	8.5e-08	1.8e-07	1.7e-07	3.82e-07	3.96e-07	7.35e-07
14.5 - 15.0	6.51e-07	7.5e-08	6.6e-08	1.1e-07	1.5e-07	3.17e-07	3.34e-07	6.00e-07
15.0 - 15.5	5.09e-07	1.2e-07	2.8e-08	1.1e-07	8.0e-08	2.44e-07	2.65e-07	4.84e-07
15.5 - 16.0	4.69e-07	3.0e-08	1.3e-07	5.5e-08	1.1e-07	2.41e-07	2.28e-07	4.13e-07

Table 1. Invariant prompt-photon yields and their uncertainties in NLO QCD.

References

- [1] M. Wilde [ALICE Collaboration], Nucl. Phys. A904-905 **2013** (2013) 573c [arXiv:1210.5958 [hep-ex]].
- [2] A. Adare *et al.* [PHENIX Collaboration], Phys. Rev. Lett. **104** (2010) 132301 [arXiv:0804.4168 [nucl-ex]].
- [3] D. G. d'Enterria and D. Peressounko, Eur. Phys. J. C **46** (2006) 451 [nucl-th/0503054] and references therein.
- [4] [ATLAS Collaboration], ATLAS-CONF-2012-051.
- [5] S. Chatrchyan *et al.* [CMS Collaboration], Phys. Lett. B **710** (2012) 256 [arXiv:1201.3093 [nucl-ex]].
- [6] P. Steinberg [ATLAS Collaboration], Nucl. Phys. A **904-905** (2013) 233c.
- [7] R. Granier de Cassagnac [CMS Collaboration], Nucl. Phys. A **904-905** (2013) 241c.
- [8] P. Aurenche, M. Fontannaz, J. -P. Guillet, E. Pilon and M. Werlen, Phys. Rev. D **73** (2006) 094007 [hep-ph/0602133].
- [9] M. Klasen, Rev. Mod. Phys. **74** (2002) 1221 [hep-ph/0206169].
- [10] G. Aad *et al.* [ATLAS Collaboration], Phys. Lett. B **706** (2011) 150 [arXiv:1108.0253 [hep-ex]].
- [11] [ATLAS Collaboration], ATLAS-CONF-2013-022.
- [12] V. Khachatryan *et al.* [CMS Collaboration], Phys. Rev. Lett. **106** (2011) 082001 [arXiv:1012.0799 [hep-ex]].
- [13] S. Chatrchyan *et al.* [CMS Collaboration], Phys. Rev. D **84** (2011) 052011 [arXiv:1108.2044 [hep-ex]].
- [14] P. K. Khandai, P. Shukla and V. Singh, Phys. Rev. C **84** (2011) 054904 [arXiv:1110.3929 [hep-ph]].
- [15] M. Klasen and G. Kramer, Phys. Lett. B **386** (1996) 384 [hep-ph/9605210].
- [16] D. Stump, J. Huston, J. Pumplin, W. -K. Tung, H. L. Lai, S. Kuhlmann and J. F. Owens, JHEP **0310** (2003) 046 [hep-ph/0303013].
- [17] N. Hammon, A. Dumitru, H. Stoecker and W. Greiner, Phys. Rev. C **57** (1998) 3292 [hep-ph/9801292].
- [18] A. Dumitru, L. Frankfurt, L. Gerland, H. Stoecker and M. Strikman, Phys. Rev. C **64** (2001) 054909 [hep-ph/0103203].
- [19] A. Adare *et al.* [PHENIX Collaboration], arXiv:1208.1234 [nucl-ex].
- [20] B. Abelev *et al.* [ALICE Collaboration], Phys. Rev. Lett. **110** (2013) 082302 [arXiv:1210.4520 [nucl-ex]].
- [21] K. J. Eskola, H. Paukkunen and C. A. Salgado, JHEP **0904** (2009) 065 [arXiv:0902.4154 [hep-ph]].
- [22] M. Hirai, S. Kumano and T. -H. Nagai, Phys. Rev. C **76** (2007) 065207 [arXiv:0709.3038 [hep-ph]].

- [23] D. de Florian, R. Sassot, P. Zurita and M. Stratmann, Phys. Rev. D **85** (2012) 074028 [arXiv:1112.6324 [hep-ph]].
- [24] I. Schienbein, J. Y. Yu, K. Kovarik, C. Keppel, J. G. Morfin, F. Olness and J. F. Owens, Phys. Rev. D **80** (2009) 094004 [arXiv:0907.2357 [hep-ph]].
- [25] L. Bourhis, M. Fontannaz and J. P. Guillet, Eur. Phys. J. C **2** (1998) 529 [hep-ph/9704447].
- [26] E. L. Berger, L. E. Gordon and M. Klasen, Phys. Rev. D **58** (1998) 074012 [hep-ph/9803387].
- [27] E. L. Berger, L. E. Gordon and M. Klasen, Phys. Rev. D **62** (2000) 014014 [hep-ph/9909446].
- [28] M. Brandt and M. Klasen, arXiv:1305.5677 [hep-ph].
- [29] I. Arsene *et al.* [BRAHMS Collaboration], Phys. Rev. Lett. **93** (2004) 242303 [nucl-ex/0403005].
- [30] A. D. Martin, R. G. Roberts, W. J. Stirling and R. S. Thorne, Eur. Phys. J. C **4** (1998) 463 [hep-ph/9803445].
- [31] A. D. Martin, W. J. Stirling, R. S. Thorne and G. Watt, Eur. Phys. J. C **63** (2009) 189 [arXiv:0901.0002 [hep-ph]].
- [32] J. Pumplin, D. R. Stump, J. Huston, H. L. Lai, P. M. Nadolsky and W. K. Tung, JHEP **0207** (2002) 012 [hep-ph/0201195].
- [33] F. Arleo, JHEP **0609** (2006) 015 [hep-ph/0601075].
- [34] S. Albino, B. A. Kniehl and R. Perez-Ramos, Nucl. Phys. B **819** (2009) 306 [arXiv:0903.4825 [hep-ph]].
- [35] N. Borghini and U. A. Wiedemann, hep-ph/0506218.
- [36] S. Albino, M. Klasen and S. Soldner-Rembold, Phys. Rev. Lett. **89** (2002) 122004 [hep-ph/0205069].
- [37] S. S. Adler *et al.* [PHENIX Collaboration], Phys. Rev. Lett. **94** (2005) 232301 [nucl-ex/0503003].
- [38] D. G. d'Enterria, nucl-ex/0302016.
- [39] B. Abelev *et al.* [ALICE Collaboration], arXiv:1301.4361 [nucl-ex].
- [40] C. E. Fink, hep-ph/0105276.
- [41] E. Laenen, G. F. Sterman and W. Vogelsang, Phys. Rev. Lett. **84** (2000) 4296 [hep-ph/0002078].
- [42] G. F. Sterman and W. Vogelsang, Phys. Rev. D **71** (2005) 014013 [hep-ph/0409234].
- [43] F. Landry, R. Brock, P. M. Nadolsky and C. P. Yuan, Phys. Rev. D **67** (2003) 073016 [hep-ph/0212159].
- [44] B. G. Zakharov, JETP Lett. **80** (2004) 1 [Pisma Zh. Eksp. Teor. Fiz. **80** (2004) 3] [hep-ph/0405101].
- [45] W. Liu and R. J. Fries, Phys. Rev. C **77** (2008) 054902 [arXiv:0801.0453 [nucl-th]].